CORA Cork Open Research Archive
Cartlann Taighde Oscailte Chorcaí

Title	Offshore wind resource in the context of global climate change over a tropical area
Authors	Vu Dinh, Quang;Doan, Quang-Van;Ngo-Duc, Thanh;Dinh, Van Nguyen;Duc, Nguyen Dinh
Publication date	2021-12-22
Original Citation	Vu Dinh, Q., Doan, Q.-V., Ngo-Duc, T., Dinh, V. N. and Duc, N. D. (2021) 'Offshore wind resource in the context of global climate change over a tropical area', Applied Energy, 308, 118369 (11pp). doi: 10.1016/j.apenergy.2021.118369
Type of publication	Article (peer-reviewed)
Link to publisher's version	10.1016/j.apenergy.2021.118369
Rights	© 2021, Elsevier Ltd. All rights reserved. This manuscript version is made available under the CC BY-NC-ND 4.0 license. - https://creativecommons.org/licenses/by-nc-nd/4.0/
Download date	2026-11-07 03:59:47
Item downloaded from	https://hdl.handle.net/10468/13166

UCC
University College Cork, Ireland
Coláiste na hOllscoile Corcaigh

Offshore wind resource in the context of global climate change over a tropical area

Quang Vu Dinh[1,2], Quang-Van Doan[3*], Thanh Ngo-Duc[4], Van Nguyen Dinh[5], Nguyen Dinh Duc[1]

[1] Department of Engineering and Technology in Constructions and Transportation, VNU-Hanoi - University of Engineering and Technology, Vietnam

[2] MaREI Centre, ERI Beaufort Building, University College Cork, Ireland

[3] Center for Computational Sciences, University of Tsukuba, Japan

[4] University of Science and Technology of Hanoi, Vietnam Academy of Science and Technology, Vietnam

[5] Offshore Wind Consultants, AqualisBraermar LOC Group, Ireland and Vietnam

*Corresponding author, email: doan.van.gb@u.tsukuba.ac.jp

Abstract:

Understanding the future offshore wind energy is crucial for making an appropriate energy strategy. Yet how offshore wind energy will respond to the rapidly intensifying global warming remains inconclusive. Focusing on a tropical sea in Vietnam, this study assesses the climatic impact of global warming on the local offshore wind potential. Dynamically downscaled wind data obtained by an edge-cutting fine-resolution regional climate model with two greenhouse-gases Representative Concentration Pathway (RCP) scenarios 8.5 and 4.5 were biased-corrected with a quantile mapping method before using for assessment. Results revealed a decreasing trend of the annual-mean offshore wind speed and power potential in Vietnam under both scenarios. However, the change is seasonally asymmetric with profound decreases of about 2 – 10% in September-October-November and slight increases of about 2 – 4% in December-January-February. The turbine-based assessment showed that the cumulative annual energy obtained from the 12 MW and 8 MW turbines could reach the highest about 50.9 GWh and 30.7 GWh (2080–2099 average under scenario RCP8.5) but the difference in their capacity factor is much smaller, suggesting that turbine 8MW should be considered in the sense of cost-effectiveness in some areas.

***Keywords*:** Wind speed, wind turbine, future offshore wind energy; bias correction; Vietnam

Introduction

Clean and renewable energies are keys to reducing fossil fuels dependency and promoting a decarbonized economy. Transition to clean and renewable energies is an essential solution to achieve the Sustainable Development Goals (regarding affordable and clean energy) toward 2030 addressed by the United Nations [1]. Offshore wind energy arises as a highly prospective renewable energy resource with great potential for growth due to the scarcity of installed offshore wind farms and the vast ocean areas available for installation. A primary advantage of offshore wind energy is the higher electricity generation ability because wind speeds over the ocean are generally steadier and stronger than over land areas [2]. Also, another plus is practically unlimited offshore sites for wind farm deployment with little or no impact on the residential conflict [2]. Moreover, recent advances in offshore wind technologies help to reduce the capital, installation and operation costs [3].

An increasing number of studies investigated the future change of wind field and respective wind energy potential with global warming [4–13]. A majority of studies is focused on onshore wind energy [6,7,10,13,14]. Fewer studies have addressed offshore wind energy [4,5,11,12]. Technically, quantitative assessment of future wind energy is conducted based on climate projection data delivered by state-of-the-art Global Climate Models (GCMs). GCMs can represent the atmospheric dynamics processes considering greenhouse gas concentration scenarios [4]. However, the coarse resolution of GCMs (about roughly 100 km or more up to date) is not desirable for assessing offshore wind potential over ocean areas close to the coastline, where wind-energy exploration is likely feasible. Downscaling approaches generate spatial-detailed wind information from GCMs outcomes, up to the scale practical for decision making. Downscaling techniques include statistical-based, some of which use machine learning algorithms [4], and dynamical downscaling (DDS) with fine-resolution regional climate models (RCM) forced by GCMs outputs. An advantage of DDS regarding its dynamic-based characteristic allows models to represent localized atmospheric physical processes explicitly, though the method demands higher computational resources [15].

Recent studies revealed understandings about future offshore wind energy potential regarding how it will change with the intensifying global warming. For instance, Zhang and Li [4] showed that future offshore wind energy (i.e., 2041–2060 and 2081–2100) would increase over the Chinese coastline in the South China Sea while decreasing over the East China Sea. Earlier studies showed the increasing signal of wind power (up to + 20 % at the end of the 21st century) over the Baltic Sea [6,7] . Meanwhile, Barstad et al. [8] showed that wind speed and wind power generation in 2020–2049 were projected to decrease slightly with a range of 2–6% when comparing to 1972–2001 in most areas of northern Europe. Koletsis et al. [9] combined six RCM simulations to evaluate future wind energy potential over the Mediterranean Sea for 2021–2050 and 2061–2090. They found out a decrease over the central Mediterranean Sea and an increase over the Alboran, Aegean seas and the Gulf of Lion. Richard et al.

[10] assessed the impact of climate change on wind energy in the two future periods 2021–2050 and 2061–2090 over the European domain. They found that wind energy resources were projected to decrease over most of Europe and increase over the Barents Sea and North Africa under two greenhouse-gases scenarios, i.e., the Representative Concentration Pathway (RCP) 4.5 and RCP 8.5.

A study gap lies in the inconclusive understanding of how future offshore wind energy will respond to the global warming effects as both increase/decrease signals are detected in the literature. Note that wind modification in response to global warming is not straightforward because of complex physical processes underlying climate systems [16,17]. Diversifying target geographical regions is needed to build comprehensive knowledge about the issue.

This study aimed to advance the current understanding of the future change in offshore wind energy potential under the global warming effects over a tropical region, taking Vietnam as a case study. The detection of global-warming signals over a tropical area like Vietnam contributes to general knowledge on the future change in offshore wind energy. Dynamically downscaled wind data are obtained from a state-of-the-art fine-resolution RCM. Two greenhouse-gases scenarios, RCP 4.5 and RCP 8.5, are considered to catch inter-scenario variability. In detail, we aim to answer two research questions in this study: (1) How does climate change influence annual and seasonal offshore wind energy in the low-latitude area? And (2) What are the new risks and opportunities of offshore wind power in the context of global warming.

2. Data and methodology

2.1 Dynamical downscaling wind product

Historical (hereinafter called HIST) and future sea-surface wind data are obtained from downscaling experiments, which are conducted under the framework of the Southeast Asia Regional Downscaling/Coordinated Regional Climate Downscaling Experiment (SEACLID/CORDEX-SEA) project [18]. The Regional Climate Model version 4.3 (RegCM4) [19] was integrated with the initial and boundary conditions taken from the CNRM-CM5.1 global climate model [20] for the reference period 1986–2005 and the future period 2006–2100 under two greenhouse-gases scenarios RCP4.5 and RCP8.5. CNRM-CM5.1 includes the atmospheric model ARPEGE-Climat (v5.2), the ocean model NEMO (v3.2), the land surface scheme ISBA and the sea ice model GELATO (v5) coupled through the OASIS (v3) system [20]. The horizontal resolution of CNRM-CM5.1 is equal to 1.4º (~150km) for the atmospheric component, while the RegCM4 downscaling experiment has a better spatial resolution of 25km. In this study, we consider that the horizontal resolution of approximately 25 km is adequate because we focus on the country-wide scale assessment. Note that though this study considers inter-scenario uncertainty (as two RCPs are used) and internal-climate variability (as long-term data are used for the assessment), the dynamical downscaling is based on a single global and regional climate model;

thus, inter-model uncertainty is not discussed here. The RegCM4 downscaling run configuration was based on the sensitivity experiments conducted by the CORDEX-SEA community [21–23]. More detailed information on the CNRM-CM5.1–RegCM4 experiment is found in [16], where the added values of the downscaled sea surface wind compared to the original CNRM-CM5.1 products were demonstrated. Although the downscaled products cover the Southeast Asian domain of [15ºS–27ºN; 89.5ºE–146.5ºE], this present study only focuses on the off-shore region of [6ºN–24ºN; 101ºE–115ºE] surrounding Vietnam.

2.2 Bias correction method

Model errors are inevitable as numerical models are not perfect [24]. Climate models exhibit systematic error (biases) due to the limited spatial resolution, simplified dynamic and physics processes, or incomplete knowledge of climate system. Hence, the raw climate model outputs have to be bias-corrected before being used for further assessment. Bias correction for wind speed has been applied for previous studies [5,8,13]. Errors from model outputs may affect study results. Using bias correction can therefore help to increase the similarity of simulation data to observed data. The quantile mapping method can make the distributions of two datasets close together. In general, the steps of the method used in this paper are as follows:

- Two parts (calibration and validation) are obtained from dividing the simulation and observed data
- The distribution function in the calibration part is determined
- Transfer function is determined
- Transfer function is applied to adjust the wind speed during the validation period
- The effectiveness of the method is evaluated based on the 95th percentiles (q95), 99th percentiles (q99), coefficient of variation (CV)

Li et al. [25] compared five bias correction methods and showed that the quantile mapping method based on the Weibull distribution (QMWD) best-corrected surface wind data. Therefore, we apply the QMWD method (Library Python scipy's exponweib) in this study for each grid point of the downscaled CNRM-CM5.1–RegCM4 product. The limitation of QMWD is that the method cannot retain intervariable dependencies and adds variability to smooth spatial fields, though it can correct any bias in the distribution function [26]. The observational wind dataset is obtained from a Cross-Calibrated Multi-Platform (CCMP) project of the National Aeronautics and Space Administration (NASA). The CCMP dataset was built by combining information from several satellite devices such as microwave scatter meters (SeaWinds, QuikScat) and microwave radiometers (WindSat, TMI, etc.). The CCMP dataset is a reliable illustration of the ocean surface wind at a temporal resolution (6-hourly) and a high spatial resolution (0.25º) from July 1987 to June 2011 [27]. This study uses the CCMP as a reference surface wind dataset for the simulation's bias correction.

The two datasets, simulation data (HIST) and CCMP, are used to correct bias and evaluate future wind energy in Vietnam. As the resolution of the two datasets is close, here we apply "nearest neighbor" interpolation approach when regridding CCMP data to CORDEX SEA coordinates before using it for bias correction. In this study, the dataset obtained after bias correcting the HIST is called the BC.

Table 1. Characteristics of datasets

	OBS	**HIST**	**BC**
Origin	NASA's Cross-Calibrated Multi-Platform (CCMP) dataset	Historical dynamical downscaling data from the Southeast Asia Regional Downscaling/Coordinated Regional Climate Downscaling Experiment (SEACLID/CORDEX-SEA)	Bias-corrected historical dynamical downscaling data from the Southeast Asia Regional Downscaling/Coordinated Regional Climate Downscaling Experiment (SEACLID/CORDEX-SEA)
Spatial coverage	Global	15ºS–27ºN; 89.5ºE–146.5ºE	6ºN–24ºN; 101ºE–115ºE
Spatial resolution (latitude x longitude)	0.25º x 0.25º	0.226º x 0.226º	0.226º x 0.226º
Temporal resolution	6-hourly	Daily	Daily

We describe the equations used for the QMWD method [25] as follows.

The Weibull distribution function used to approximate wind data is:

$$WDf(V) = \left(\frac{V}{c}\right)^{k-1} \times \frac{k}{c} \times e^{-\left(\frac{V}{c}\right)^{k}} \qquad (1)$$

where k, c are shape and scale parameters, respectively. V is surface wind velocity.

The Weibull distribution's cumulative distribution function is:

$$f(V) = 1 - e^{-\left(\frac{V}{c}\right)^{k}} \qquad (2)$$

Then the following transfer function is applied to transform the HIST simulated wind speed into the BC data whose distribution is close to that of the observed data:

$$V_{BC} = f_{OBS}^{-1}\left(f_{HIST}(V_{HIST})\right) = c_{OBS}\left[-ln\left(1 - \left(1 - e^{-(V_{HIST}/c_{HIST})^{k_{HIST}}}\right)\right)\right]^{1/k_{OBS}} \qquad (3)$$

where the subscripts "$_{OBS}$", "$_{HIST}$" and "$_{BC}$" denote the CCMP data, simulation data and the data after bias correction, respectively.

2.3 Wind power calculation

Since wind speed generally increases with height, the hub height of the wind turbines is designed to be at a high altitude to generate more electrical power [28]. Thus, to estimate wind power potential, there is a need to extrapolate surface wind speed to the values at the turbine hub height. The two most common

analytical methods for extrapolating wind speed with altitude are log and power laws [29]. The power law method [8,30,31], which represents the wind speed relationship between different heights in the simplest way, is applied in this study:

$$V_{hub} = V_{surface}\left(\frac{z_{hub}}{z_{surface}}\right)^{\alpha} \quad (4)$$

where z is altitude, V is wind velocity. The subscripts "hub" and "surface" denote the turbine hub height and surface level ($z_{surface}$=10m), respectively. α is the power law exponent, depending on many factors such as environmental conditions, local climatology and surface roughness. In this study, the value α =1/10 is chosen following previous works [8,30,31].

There are currently two popular types of turbines, i.e., the horizontal- and vertical-axis wind turbines, where the former is more common than the latter. In this study, the reference horizontal axis turbines for an offshore wind farm are assumed to be Haliade-X 12MW (HX12) and MHI Vestas V164 8MW (VS8). At a time *t*, the power generated by the wind turbines is determined according to the formula below [32]:

$$P_{turbine}(t) = \begin{cases} 0, & V(t) < v_{cut\,in} \\ 0.5 \times \rho_{air} \times C_p \times A_t \times V(t)^3, & v_{cut\,in} \le V(t) < v_{rate} \\ P_{rate}, & v_{rated} \le V(t) < v_{cut\,off} \\ 0, & v_{cut\,off} \le V(t) \end{cases} \quad (5)$$

where $C_p = 0.35$ is the power curve coefficient and $\rho_{air} = 1.225\ kg/m^3$ is air density

Table 2. Characteristics of the turbines

Characteristics	**Haliade-X 12** [33]	**MHI Vestas V164** [34,35]
Rated power (P_{rate})	12000 kW	8000 kW
Rotor diameter (D_r) **(m)**	218.2	164
Cut-in velocity $(v_{cut\,in})$ **(m/s)**	3.5	4
Rated velocity (v_{rated}) **(m/s)**	12	13
Cut-out velocity $(v_{cut\,off})$ **(m/s)**	28	25

The energy output of the wind turbine during the period is:

$$E_{out} = \sum_{t=1}^{N} P_{turbine}(t) \times T_r \quad (6)$$

where T_r and *N* are the temporal resolution (in hours) and the number of spans, respectively.

The capacity factor (CF), i.e. the efficiency of the wind turbine, represents the ratio between the total energy output and the maximum energy output of the turbine over a time period, usually a year [20]. It is determined by the following formula:

$$CF = \frac{E_{out}}{\sum_{t=1}^{N} P_{rated} \times T_r} \times 100\% \qquad (7)$$

Fig. 1 displays the relationship between the velocity and power output of HX12 and VS8 wind turbines. Similarly to Dinh and Nguyen [36], this study assumes that the wind farm has a density of one turbine per one square kilometer.

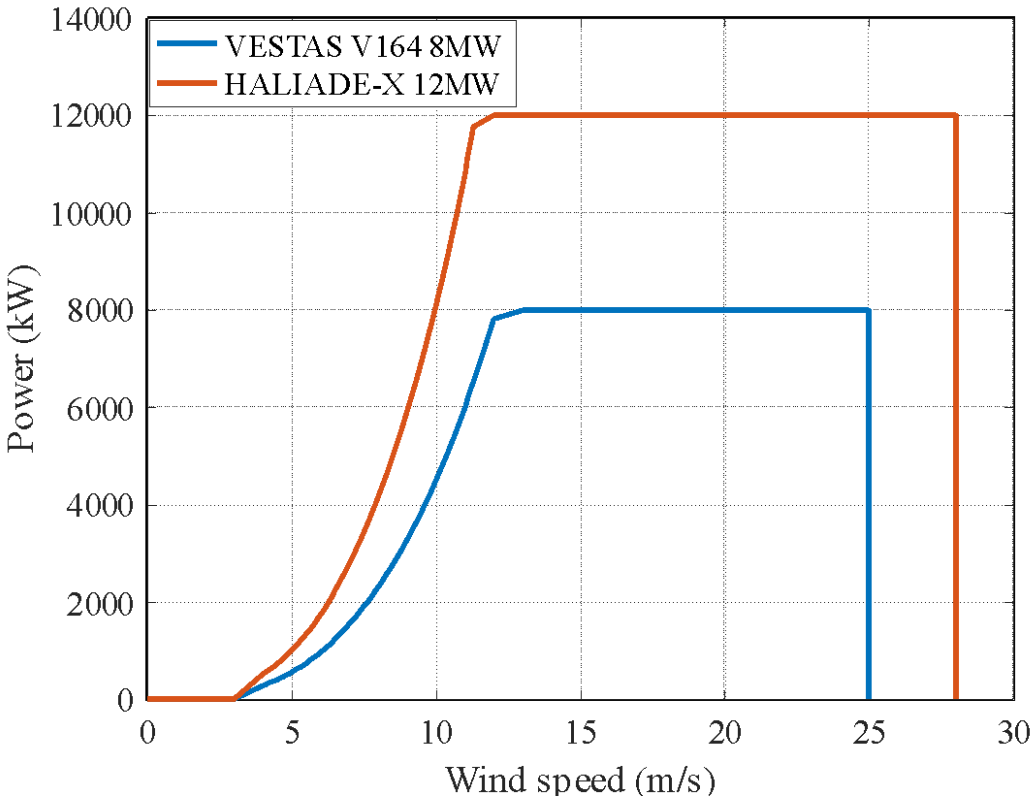


Figure 1. Power curve of HX12 ([33]) and VS8 ([34,35]) turbines

3. Results and discussions

3.1 Bias correction

Applying the QMWD approach described in Section 2.2, the transfer function is derived at each grid point for the training period 1988–2000. The independent period 2001–2005 is used to evaluate the effectiveness of the transfer function. Fig. 2(a, c) shows that the BC annual wind speed obtained after applying the QMWD method is close to the observed data. When comparing Fig. 2(a, b), we see a relatively large difference between the HIST and the OBS datasets. Accordingly, the absolute bias of

the BC with the reference OBS data is significantly lower than the HIST's mean bias (0.0 m/s versus 1.89 m/s and -0.12 m/s versus 1.78 m/s over the training period 1988–2000 and the independent period 2001–2005, respectively). After the correction, the mean biases become small of approximately -0.12 m/s (2 ~ 3 %) as shown in Fig. 2(e-2), that is consistent to the results of Li et.al [25] for the region of interest (Vietnam). Fig 2(f, g) shows the Root Mean Square Error (RMSE) of HIST and BC compared with OBS data. The mean RMSE value decreased from 2.49 to 1.3 over the independent period after applying the bias correction. In addition, bias correction used in this research is good because RMSE over the independent period is quite similar to the training period.

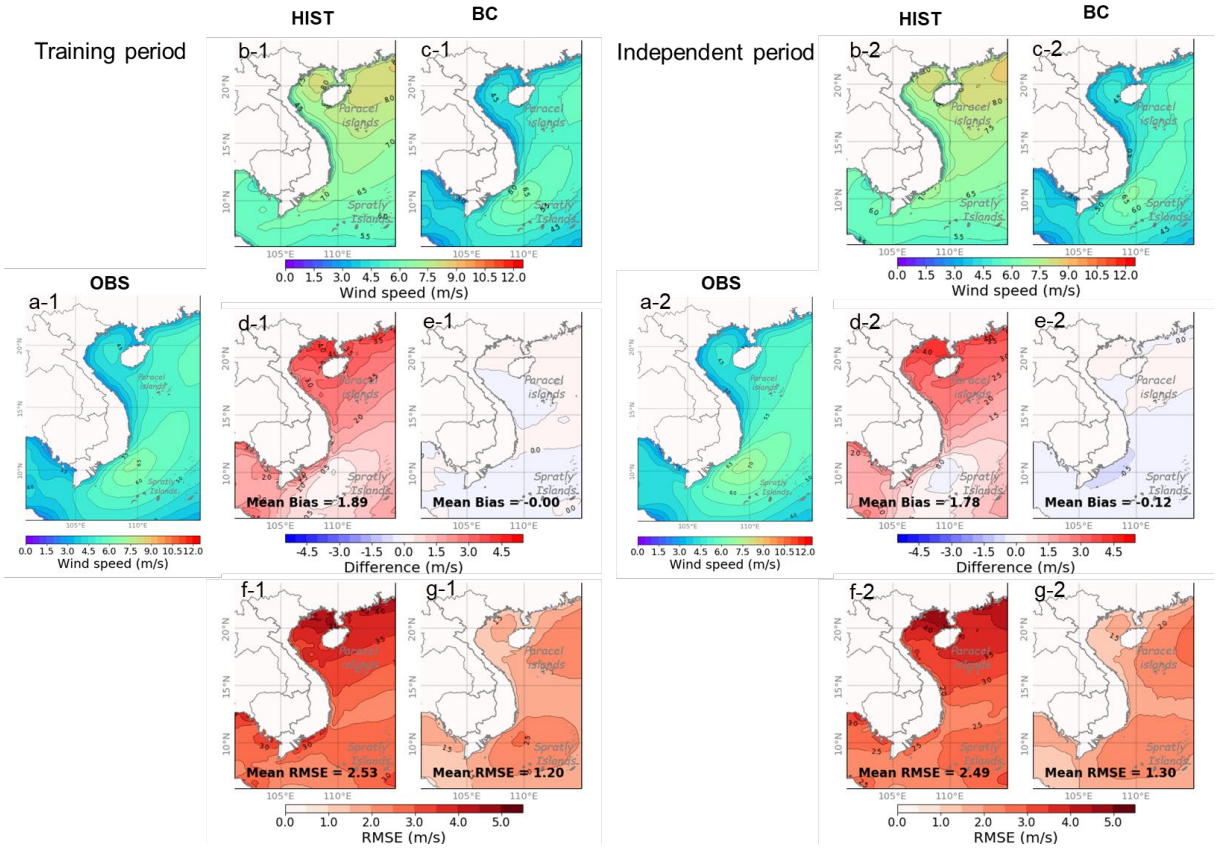


Figure 2. (a-c) annual-mean surface wind speed of a) the CCMP-observed data (OBS), b) the SEACLID/CORDEX-SEA dynamically downscaled data (HIST), c) the BC data; and the difference between d) the HIST, e) the BC and OBS; Root Mean Square Error between f) the HIST, g) the BC and OBS over the training period 1988–2000 (left,1) and the independent period 2001–2005 (right, 2).

Fig. 3 illustrates the 95th percentiles (q95), 99th percentiles (q99) and coefficient of variation (CV) of three datasets during 1988–2000 and 2001–2005. Overall, we can confirm the high similarities between the BC and OBS. The mean q95 of the HIST is 9.3 m/s, while those of OBS and the BC are 5.33 m/s and 5.46 m/s over the independent period, respectively. The mean q99 value obtained from the HIST (11.19 m/s) is almost double that obtained from OBS (5.76 m/s) and the BC (6.5 m/s). The spatial distribution of the BC's CV is quite similar to that of OBS. In addition, the mean CV also shows the similarity of the BC (mean CV 45.97 %) and OBS (mean CV 46.18 %) while the HIST's mean CV is

50.65 % in Fig. 3(g1-i1). Fig. 2 and Fig. 3 also show the largest discrepancy between OBS and HIST in the northern area.

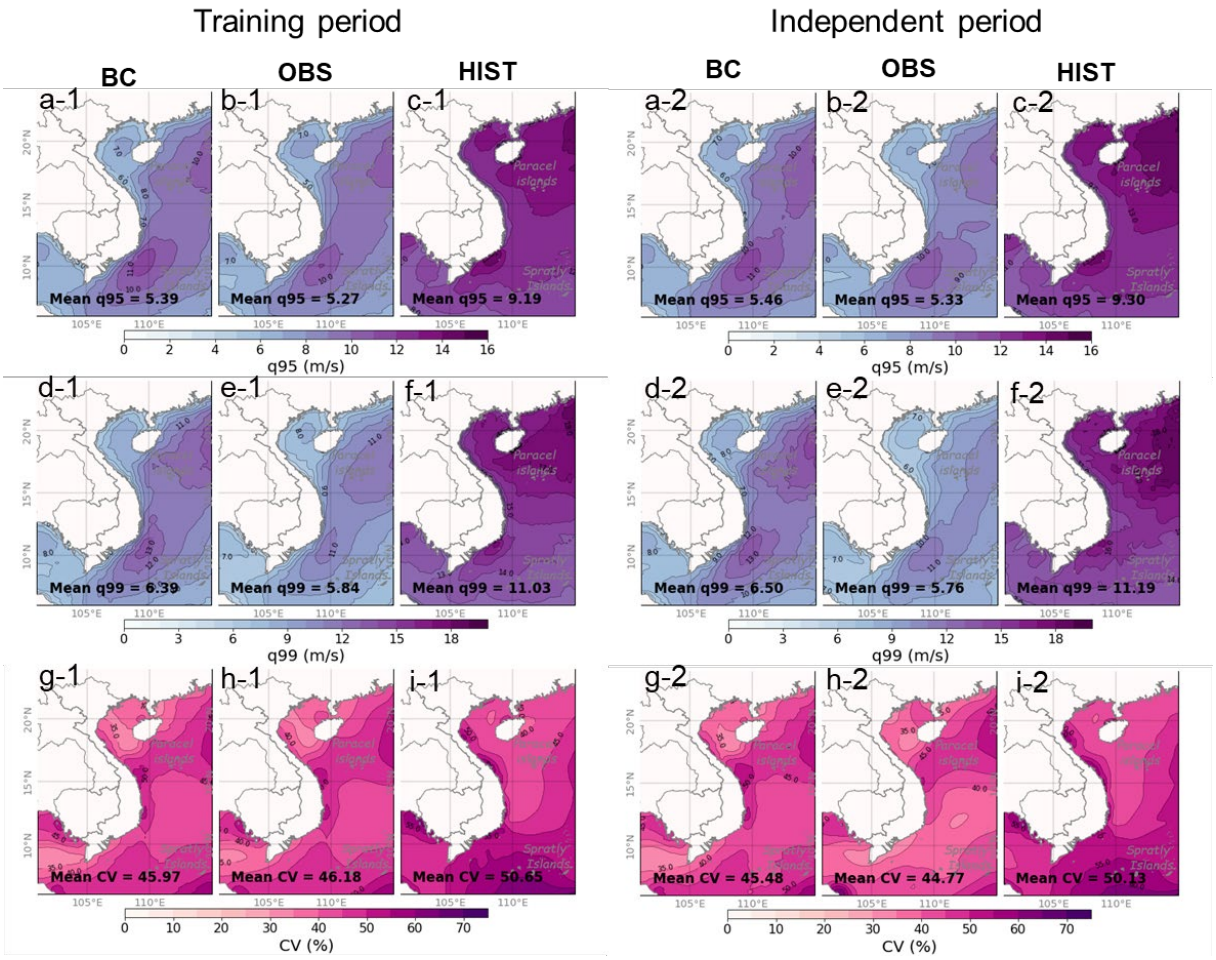


Figure 3. (a1–c1, a2–c2) 95th percentiles, (d1–f1, d2–f2) 99th percentiles and (g1–i1, g2–i2) coefficient of variation of the BC, OBS, and HIST over the training period 1988–2000 (left, 1) and the independent period 2001–2005 (right, 2)

To illustrate how the QMWD method modifies the data probability distribution, Fig. 4(a–e) compares the wind speed distribution of the three datasets over the periods 1988–2000 and 2001–2005 at five points offshore of Vietnam (Fig. 4f). Vietnam has a long coastline, so the five points selected are also five islands near the shore which are also evenly spaced along the coastline. The study used the Kolmogorov-Smirnov (KS) method to test the adequacy of the Weibull distribution function. Fig. 4(g–k) show Weibull distribution and Kolmogorov-Smirnov's p–value for BC data over independent period. The p-value obtained from the KS test greater than 0.05 shows a high similarity between the data and the distribution function. Combining KS p–values at 5 selected points (>0.05) with the histograms, it can be seen that the Weibull function used in the study is completely suitable. The HIST distribution differs significantly from that of the reference data. The HIST distributions for all five points are flatter and more concentrated at higher wind speed values than OBS. After applying the QMWD method, the

probability distributions of the BC data almost coincide with the OBS distribution for the training period. The BC distribution is also primarily improved compared to the HIST one over the independent period 2001–2005. However, slight differences in phase and amplitude with OBS are noticed (e.g. at point 4).

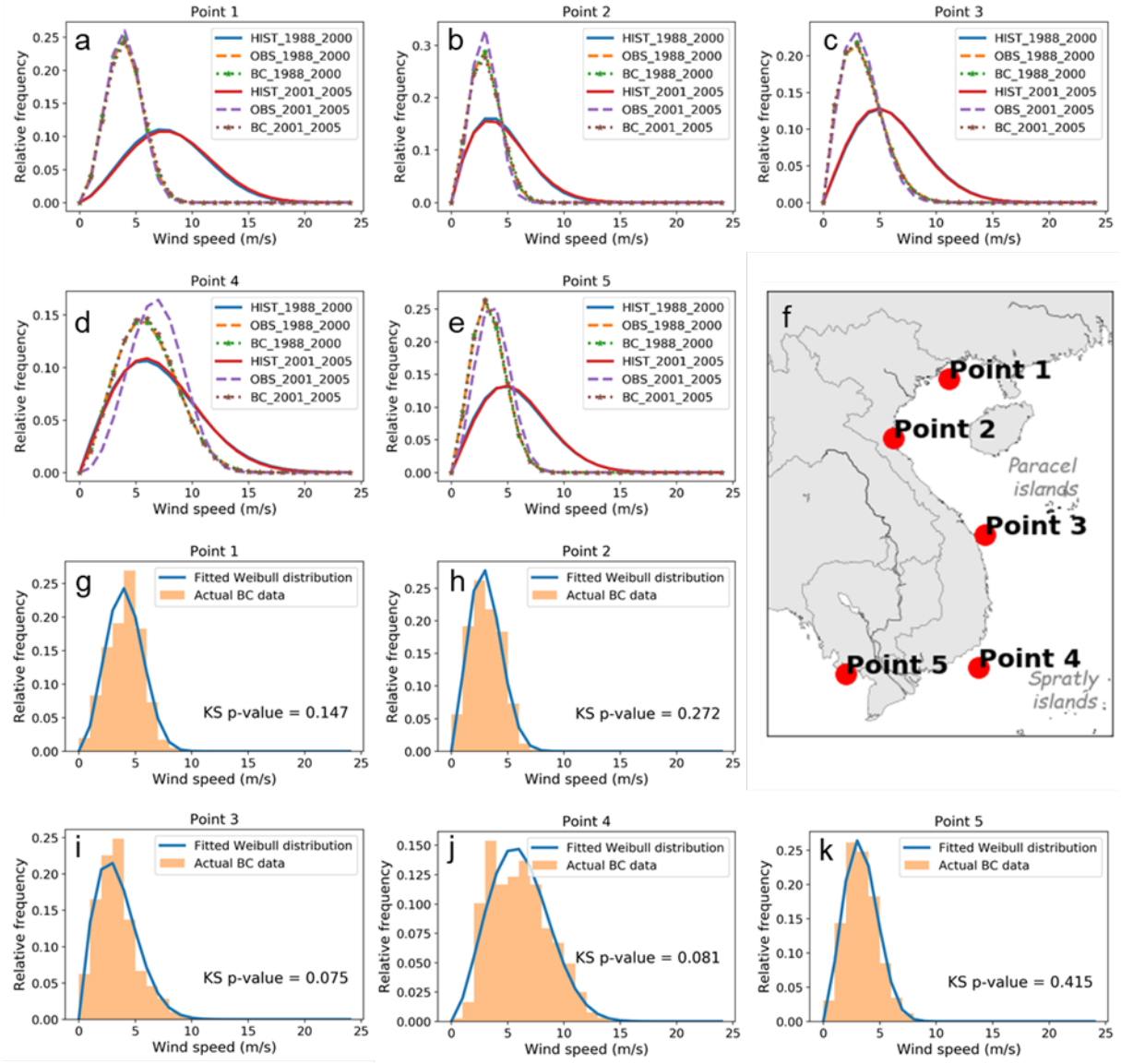


Figure 4. Wind speed probability distribution of the OBS, HIST and BC datasets at 5 selected points for the training period 1988–2000 and the independent period 2001–2005.

The results shown above indicate that the application of the QMWD method has significantly improved the model surface wind field. To maximize the construction period for having a better transfer function [37,38], the entire test period 1988–2005 is used to infer new transfer functions applied to the future wind data at each grid point. Next, the BC future surface wind is extrapolated to the turbine hub height following Equation (4) and analyzed below.

3.2 Future changes in wind speed

Fig. 5 shows the wind speed changes at the turbine hub height between the mid- and far-future periods under two scenarios, RCP4.5 and RCP8.5, with the reference period 1988–2005. Overall, wind speed is projected to slightly decrease in the future except in the southern offshore area. This agrees with the study of Herrmann et al. [16] where the weakening of projected surface wind speed was shown to be due to the increase of mean meridional south to north sea level pressure gradient over the Southeast Asian oceanic region. The reduction of offshore wind speed is more pronounced in the south central offshore areas. Especially, the offshore areas of Ninh Thuan and Binh Thuan provinces (around point 4 in Fig. 4f with coordinates of 12ºN, 109ºE) are the regions with the largest decrease (about 4–7%) in future wind speed in Vietnam. However, it is worth mentioning that Ninh Thuan and Binh Thuan offshore areas are still the regions with the highest annual average wind speed in the reference period (Fig.5a) and the future (not shown). In the north of Vietnam, the Gulf of Tonkin remains the region with the highest future annual wind speed. Future offshore wind speed in northern Vietnam is projected to decrease by about 2–3%.

In contrast, future wind speed in the southern offshore area is projected to increase. The offshore area of Vietnam with a latitude less than 10.9ºN is forecast to increase wind speed in the future with the range of 0–5m/s and 0–9 m/s under RCP4.5 and RCP8.5, respectively. The magnitude of increase/decrease trends in offshore wind speed is more enhanced in the far-future period than in the mid-future and more under RCP8.5 than under RCP4.5.

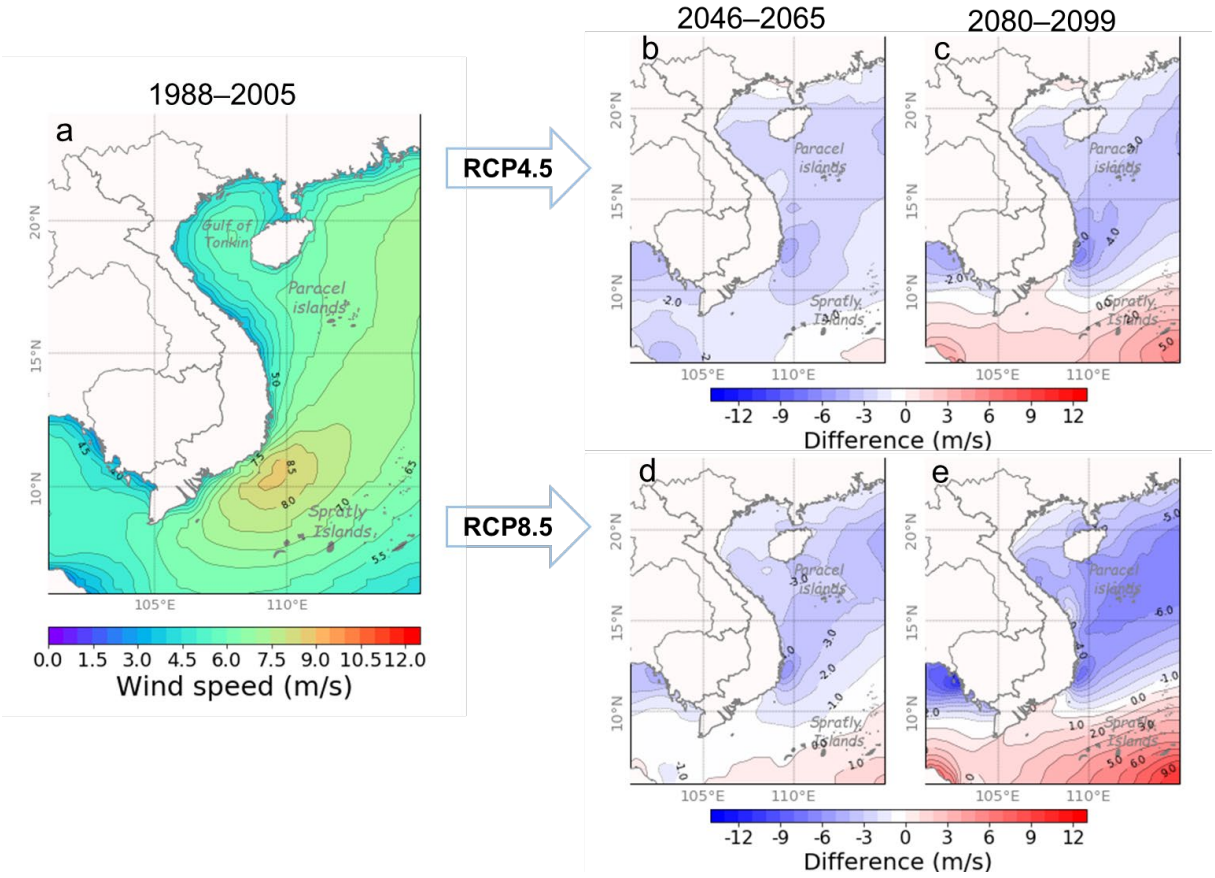


Figure 5. BC wind speed at the turbine hub height for the reference period 1988–2005 (left) and changes between the mid-future period 2046–2065 and the far-future period 2080–2099 compared to the reference period under RCP4.5 (right, upper figures) and RCP8.5 (right, lower figures).

Fig. 6 shows seasonal wind speed at the turbine's hub height over the training period 1988–2005 and the difference of seasonal wind speed between the period 2080 – 2099 under the scenario RCP8.5 and the training period. The four seasons in Fig. 6 are the months from December to February (DJF), from March to May (MAM), from June to August (JJA), and from September to November (SON). As Vietnam is located in the tropical monsoon region, wind speed thus has apparent seasonal variations. In offshore Vietnam, DJF is the season with the highest average wind speed. Wind speed at the turbine hub height can reach about 12 m/s in the offshore area of the south-central coast.

Meanwhile, the north and north-central coast areas have an average DJF wind speed of only about 4–6 m/s, which is much lower than other areas. The northern and southern areas have the lowest wind speed in MAM and JJA, respectively. Under RCP8.5 (Fig. 6, right), SON wind speed is projected to decrease by 2–10% over the whole Vietnam Sea. The reduction of offshore wind speed in both the central and northern seas and an increase in the south occur from June to August. Future offshore wind speed in the southern and north seas is projected to increase in DJF and MAM.

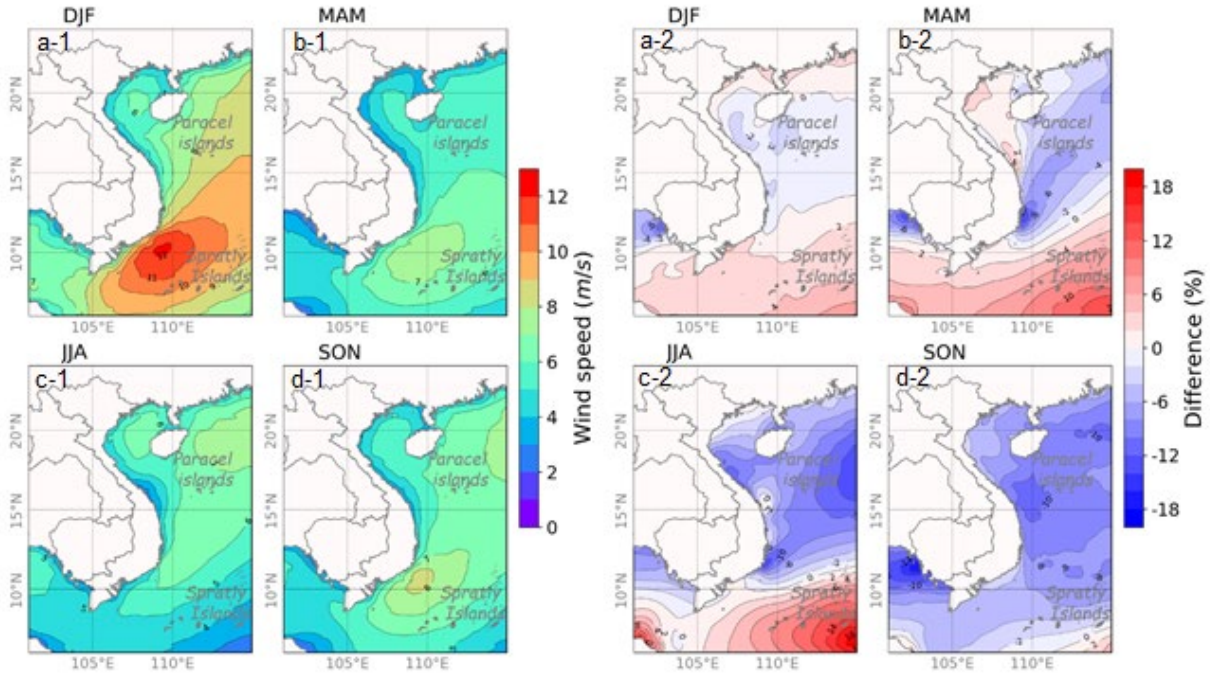


Figure 6. Seasonal wind speed average at the hub height of the test period and difference with period 2080–2099 of scenario RCP8.5.

3.3 Estimation of wind energy density

Choosing the correct type of turbine is also very important for a wind power project. Fig. 7 displays the annual offshore wind energy estimated based on the reference HX12 turbine (Fig. 7a), the energy difference between the VS8 and HX12 turbines (Fig. 7b) and the annual energy obtained with the two turbines types at five points identified in Fig.4f (Fig.7c). These values are computed for the far-future period 2080–2099 under the scenarios RCP4.5 and RCP8.5. Typically, more giant turbines (i.e. HX12M) generate more electricity. Overall, we can see that the south-central and southern seas have much greater wind energy than the northern regions (Fig. 7a). The difference in obtained wind energy from the two types of turbines is proportional to the wind speed in that area. Accordingly, wind energy at point 4 is the largest among the five selected points, at which energy obtained from the HX12 and VS8 turbines under the scenario RCP8.5 are 44.2 GWh and 26.7 GWh, respectively (Fig. 7c). At points 1, 3, and 5, the wind energy obtained under scenario RCP4.5 is higher than scenario RCP8.5. Over the whole domain, the cumulative annual wind energy for the HX12 and VS8 turbines can reach 50.9 GWh and 30.7 GWh in 2080–2099 under the scenario RCP8.5, respectively.

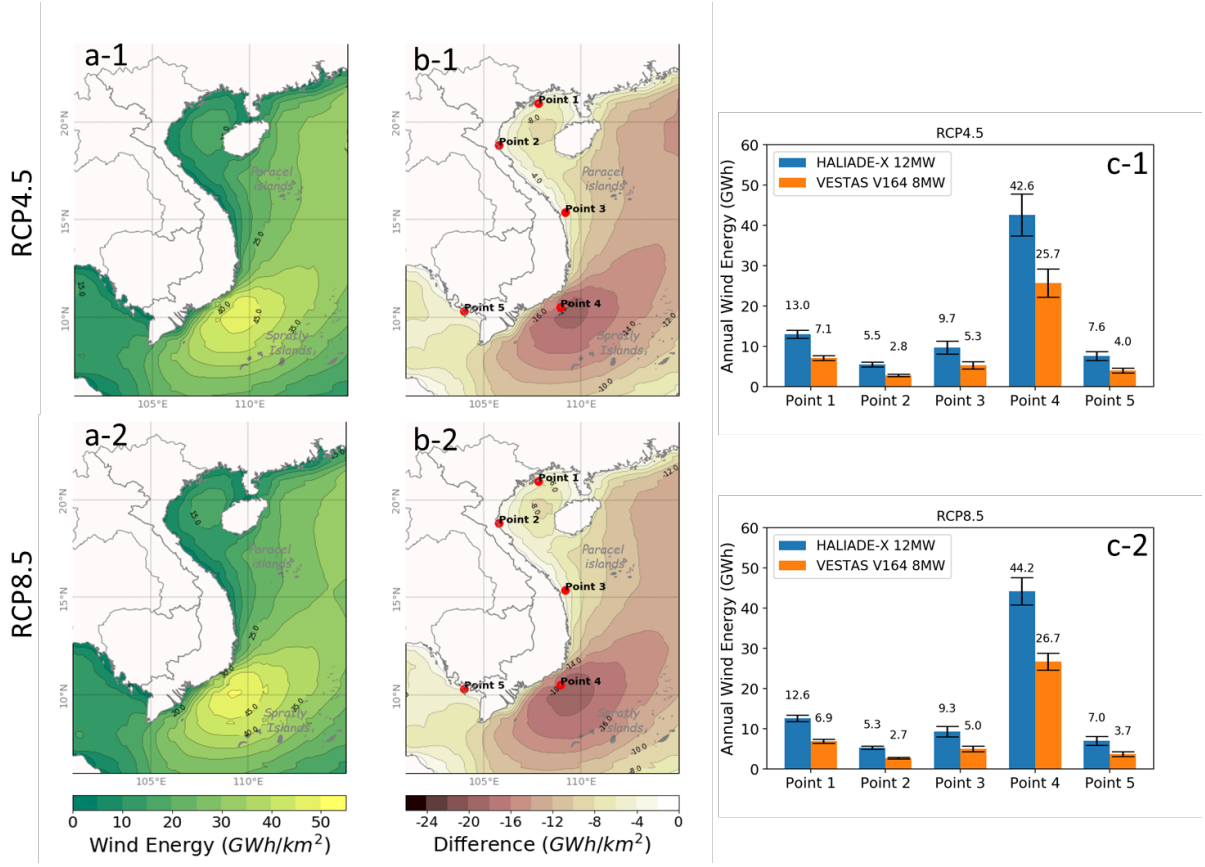


Figure 7. (a1, a2) Annual wind energy density by HX12, (b1, b2) difference wind energy between VS8 and HX12, and (c1, c2) annual wind energy production at five locations identified in Fig.4f. The values are computed for the period 2080–2099 under the scenarios RCP4.5 and RCP8.5.

3.4 Capacity factor

The annual capacity factor of the HX12 turbine for the period 2080–2099 under the scenarios RCP4.5 and RCP8.5 is shown in Fig. 8(a). The annual capacity factor of the HX12 turbine can reach about 45% in the south-central and southern seas. In the offshore areas of the north and north-central coast, the difference in the capacity factor of the two types of turbines is only about 2% (Fig. 8b). Such a slight difference suggests that an 8MW turbine should be considered when estimating the cost-effectiveness of a wind power project in these areas. The annual capacity factor obtained from HX12 and VS8 is the largest at point 4 among the five selected points, at which the capacity factor obtained from HX12 and VS8 under the scenarios RCP4.5 and RCP8.5 are (40.6%, 36.7%) and (42%, 38%), respectively (Fig. 8c).

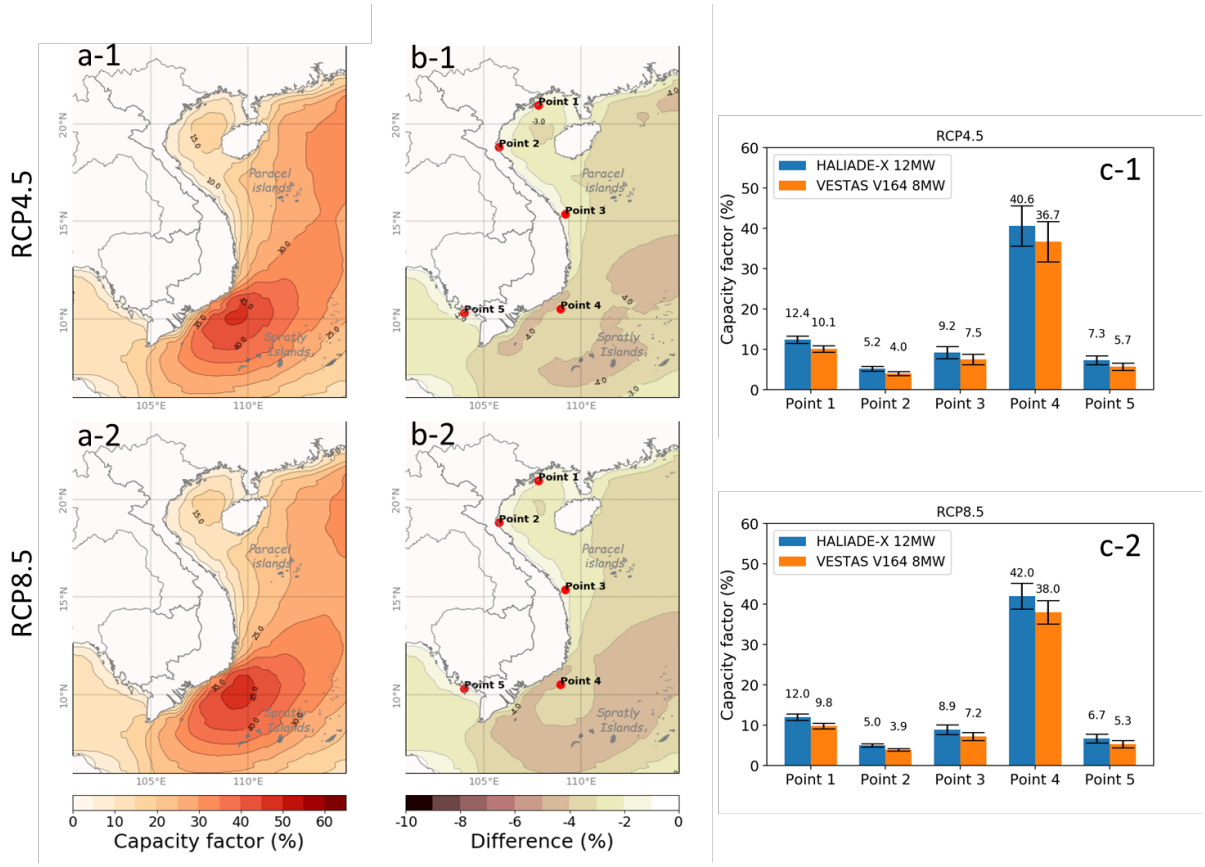


Figure 8. As in Figure 7, but for capacity factor instead of wind energy.

Fig. 9 displays the seasonal capacity factor of the HX12 turbine for the far-future periods of 2080–2099. Overall, the capacity factor of the turbine is slightly different in the two periods. The capacity factor in the southern offshore area of Vietnam is much higher than that in the north. The offshore areas of Ninh Thuan and Binh Thuan provinces have the largest capacity factor, which is projected to reach more than 80% in the DJF months of 2080–2099 under two scenarios. During JJA, the turbine in these areas operates with the lowest capacity factor with a maximum value of only about 20%. This period of the year is thus recommended for wind turbine maintenance.

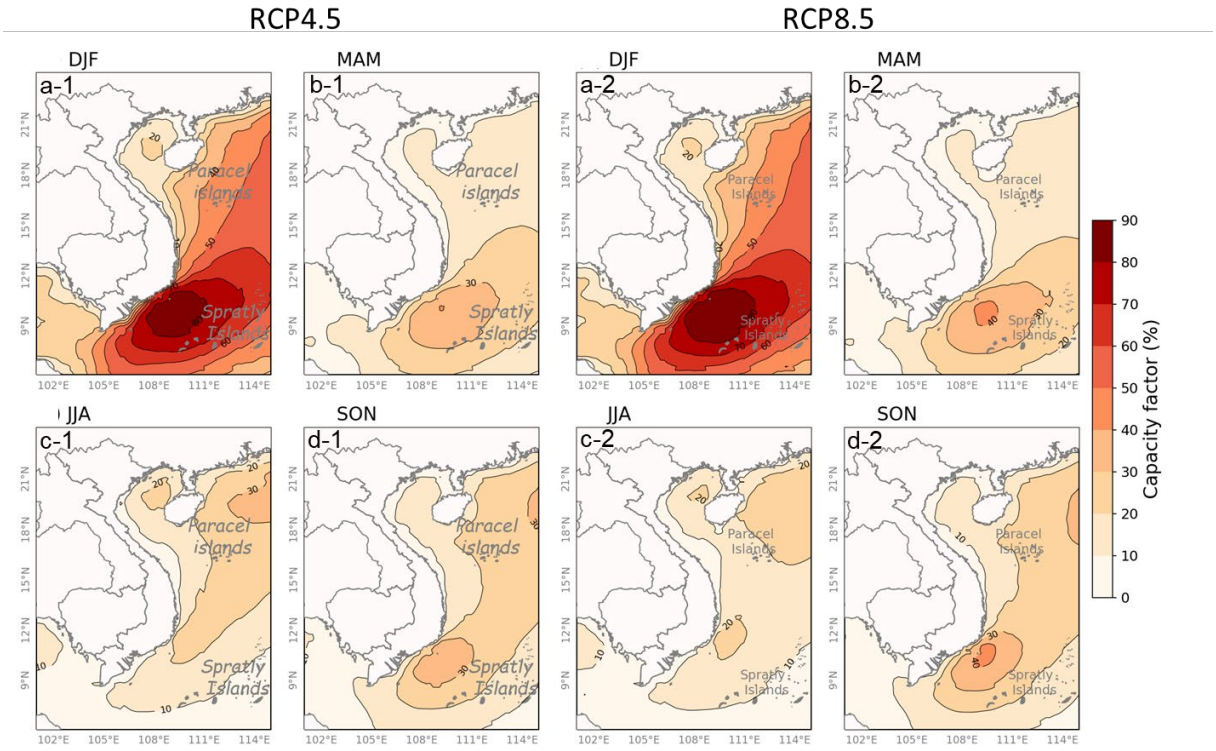


Figure 9. Seasonal capacity factor of HX12 under the scenario RCP4.5 (left, 1) and under RCP8.5 (right, 2) for the far-future period 2080–2099.

4. Conclusion

This study assesses the global-warming-associated offshore wind resource changes in Vietnam up to the middle (2046–2065) and the end of this century (2080–2099) under two greenhouse gases scenarios, RCP4.5 and RCP8.5. Dynamical downscaling data with the state-of-the-art fine-scale regional climate model is used to investigate the primary impacts of global warming on wind power potential. For the sake of reliability, modelled data has been bias-corrected using the QMWD method. The obtained results are summarized as below:

- Wind speed in most offshore regions of Vietnam is projected to slightly decrease in the future, with pronounced decreases in the south central areas such as Ninh Thuan and Binh Thuan provinces. It is worth mentioning that these offshore areas are also the areas with the highest projected annual average wind speed. SON wind speed is projected to decrease between 2 and 10% over the whole Vietnam Sea. The largest changes occur in JJA with a reduction of offshore wind speed in both the central and northern seas and an increase in the south. Future offshore wind speed in the southern and north seas is projected to increase in DJF and MAM.

- Wind energy production in the future is estimated based on actual wind turbine parameters. In particular, the study investigated the difference between Haliade-X 12MW and MHI Vestas V164 8MW turbines, which provided information for the choice of turbines for wind farms. Wind energy obtained from the two types of turbines installed in an area is proportional to the average wind speed in that area. The cumulative annual wind energy for the HX12 and VS8 turbines can reach 50.9 GWh and 30.7 GWh in 2080–2099 under the scenario RCP8.5, respectively. In the future, the capacity factor, i.e. the efficiency of wind turbines, can reach about 40–50% for the annual average and more than 80% for the DJF months in the south-central region. The lowest capacity factor of less than 20% is obtained in JJA, suggesting that JJA could be a reasonable period for wind turbine maintenance.
- The choice of turbines affects many aspects of a wind power project, such as maintenance, grid stability, and effective energy production. As the difference in capacity factor of the two types of turbines is small (about 2%) in the offshore areas of the north and north-central coast, 8MW turbines could be considered when estimating the cost-effectiveness of a wind power project in the regions.

Acknowledgements

Quang Vu Dinh has been supported in part by a research grant from the Science Foundation Ireland (SFI) under Grant No. 12/RC/2302 – P2. Thanh Ngo-Duc is supported by the Vietnam National Foundation for Science and Technology Development (NAFOSTED). Van Nguyen Dinh was formerly with the University College Cork MaREI Centre in Ringaskiddy, Co. Cork, Ireland, was supported in part by a research grant from the Science Foundation Ireland (SFI) under Grant No. 12/RC/2302 – P2, and is currently supported by OWC. However, the content of the publication herein is the sole responsibility of the authors and does not necessarily represent the views of OWC.

References

[1] United Nations, Sustainable development goals. Retrieved January 23, 2020, (2020).

[2] V.N. Dinh, E. McKeogh, Offshore Wind Energy: Technology Opportunities and Challenges BT - Proceedings of the 1st Vietnam Symposium on Advances in Offshore Engineering, in: M.F. Randolph, D.H. Doan, A.M. Tang, M. Bui, V.N. Dinh (Eds.), Springer Singapore, Singapore, 2019: pp. 3–22.

[3] H. Díaz, C. Guedes Soares, Review of the current status, technology and future trends of offshore wind farms, Ocean Eng. 209 (2020) 107381. doi:https://doi.org/10.1016/j.oceaneng.2020.107381.

[4] S. Zhang, X. Li, Future projections of offshore wind energy resources in China using CMIP6 simulations and a deep learning-based downscaling method, Energy. (2020) 119321. doi:https://doi.org/10.1016/j.energy.2020.119321.

[5] X. Costoya, A. Rocha, D. Carvalho, Using bias-correction to improve future projections of offshore wind energy resource: A case study on the Iberian Peninsula, Appl. Energy. 262 (2020) 114562. doi:https://doi.org/10.1016/j.apenergy.2020.114562.

[6] D. Carvalho, A. Rocha, M. Gómez-Gesteira, C. Silva Santos, Potential impacts of climate change on European wind energy resource under the CMIP5 future climate projections, Renew. Energy. 101 (2017) 29–40. doi:https://doi.org/10.1016/j.renene.2016.08.036.

[7] I. Tobin, R. Vautard, I. Balog, F.-M. Bréon, S. Jerez, P.M. Ruti, F. Thais, M. Vrac, P. Yiou, Assessing climate change impacts on European wind energy from ENSEMBLES high-resolution climate projections, Clim. Change. 128 (2015) 99–112. doi:https://doi.org/10.1007/s10584-014-1291-0.

[8] I. Barstad, A. Sorteberg, M. dos-S. Mesquita, Present and future offshore wind power potential in northern Europe based on downscaled global climate runs with adjusted SST and sea ice cover, Renew. Energy. 44 (2012) 398–405. doi:https://doi.org/10.1016/j.renene.2012.02.008.

[9] I. Koletsis, V. Kotroni, K. Lagouvardos, T. Soukissian, Assessment of offshore wind speed and power potential over the Mediterranean and the Black Seas under future climate changes, Renew. Sustain. Energy Rev. 60 (2016) 234–245. doi:https://doi.org/10.1016/j.rser.2016.01.080.

[10] R. Davy, N. Gnatiuk, L. Pettersson, L. Bobylev, Climate change impacts on wind energy potential in the European domain with a focus on the Black Sea, Renew. Sustain. Energy Rev. 81 (2018) 1652–1659. doi:https://doi.org/10.1016/j.rser.2017.05.253.

[11] X. Costoya, M. deCastro, D. Carvalho, M. Gómez-Gesteira, On the suitability of offshore wind energy resource in the United States of America for the 21st century, Appl. Energy. 262 (2020)

114537. doi:https://doi.org/10.1016/j.apenergy.2020.114537.

[12] D.C.A. Lima, P.M.M. Soares, R.M. Cardoso, A. Semedo, W. Cabos, D. V Sein, The present and future offshore wind resource in the Southwestern African region, Clim. Dyn. 56 (2021) 1371–1388. doi:https://doi.org/10.1007/s00382-020-05536-4.

[13] J. Moemken, M. Reyers, H. Feldmann, J.G. Pinto, Future Changes of Wind Speed and Wind Energy Potentials in EURO-CORDEX Ensemble Simulations, J. Geophys. Res. Atmos. 123 (2018) 6373–6389. doi:https://doi.org/10.1029/2018JD028473.

[14] L. Chen, Impacts of climate change on wind resources over North America based on NA-CORDEX, Renew. Energy. 153 (2020) 1428–1438. doi:https://doi.org/10.1016/j.renene.2020.02.090.

[15] F.J. Tapiador, A. Navarro, R. Moreno, J.L. Sánchez, E. García-Ortega, Regional climate models: 30 years of dynamical downscaling, Atmos. Res. 235 (2020) 104785. doi:https://doi.org/10.1016/j.atmosres.2019.104785.

[16] M. Herrmann, T. Ngo-Duc, L. Trinh-Tuan, Impact of climate change on sea surface wind in Southeast Asia, from climatological average to extreme events: results from a dynamical downscaling, Clim. Dyn. 54 (2020) 2101–2134. doi:https://doi.org/10.1007/s00382-019-05103-6.

[17] G.S. Wiser, R., Z. Yang, M. Hand, O. Hohmeyer, D. Infi eld, P. H. Jensen, V. Nikolaev, M. O'Malley, A. Zervo, Wind Energy. In IPCC Special Report on Renewable Energy Sources and Climate Change Mitigation, Cambridge, United Kingdom and New York, NY, USA, 2011. https://www.ipcc.ch/site/assets/uploads/2018/03/Chapter-7-Wind-Energy-1.pdf.

[18] F. Tangang, J.X. Chung, L. Juneng, Supari, E. Salimun, S.T. Ngai, A.F. Jamaluddin, M.S.F. Mohd, F. Cruz, G. Narisma, J. Santisirisomboon, T. Ngo-Duc, P. Van Tan, P. Singhruck, D. Gunawan, E. Aldrian, A. Sopaheluwakan, N. Grigory, A.R.C. Remedio, D. V Sein, D. Hein-Griggs, J.L. McGregor, H. Yang, H. Sasaki, P. Kumar, Projected future changes in rainfall in Southeast Asia based on CORDEX–SEA multi-model simulations, Clim. Dyn. 55 (2020) 1247–1267. doi:https://doi.org/10.1007/s00382-020-05322-2.

[19] F. Giorgi, E. Coppola, F. Solmon, L. Mariotti, M.B. Sylla, X. Bi, N. Elguindi, G.T. Diro, V. Nair, G. Giuliani, RegCM4: model description and preliminary tests over multiple CORDEX domains, Clim. Res. 52 (2012) 7–29.

[20] A. Voldoire, E. Sanchez-Gomez, D. Salas y Mélia, B. Decharme, C. Cassou, S. Sénési, S. Valcke, I. Beau, A. Alias, M. Chevallier, M. Déqué, J. Deshayes, H. Douville, E. Fernandez, G. Madec, E. Maisonnave, M.-P. Moine, S. Planton, D. Saint-Martin, S. Szopa, S. Tyteca, R. Alkama, S. Belamari, A. Braun, L. Coquart, F. Chauvin, The CNRM-CM5.1 global climate model:

description and basic evaluation, Clim. Dyn. 40 (2013) 2091–2121. doi:https://doi.org/10.1007/s00382-011-1259-y.

[21] L. Juneng, F. Tangang, J.X. Chung, S.T. Ngai, T.W. Tay, G. Narisma, F. Cruz, T. Phan-Van, T. Ngo-Duc, J. Santisirisomboon, Sensitivity of Southeast Asia rainfall simulations to cumulus and air-sea flux parameterizations in RegCM4, Clim. Res. 69 (2016) 59–77.

[22] T. Ngo-Duc, F.T. Tangang, J. Santisirisomboon, F. Cruz, L. Trinh-Tuan, T. Nguyen-Xuan, T. Phan-Van, L. Juneng, G. Narisma, P. Singhruck, Performance evaluation of RegCM4 in simulating extreme rainfall and temperature indices over the CORDEX-Southeast Asia region, Int. J. Climatol. 37 (2017) 1634–1647.

[23] F.T. Cruz, G.T. Narisma, J.B. Dado, P. Singhruck, F. Tangang, U.A. Linarka, T. Wati, L. Juneng, T. Phan-Van, T. Ngo-Duc, Sensitivity of temperature to physical parameterization schemes of RegCM4 over the CORDEX-Southeast Asia region, Int. J. Climatol. 37 (2017) 5139–5153.

[24] I. Staffell, S. Pfenninger, Using bias-corrected reanalysis to simulate current and future wind power output, Energy. 114 (2016) 1224–1239. doi:https://doi.org/10.1016/j.energy.2016.08.068.

[25] D. Li, J. Feng, Z. Xu, B. Yin, H. Shi, J. Qi, Statistical Bias Correction for Simulated Wind Speeds Over CORDEX-East Asia, Earth Sp. Sci. 6 (2019) 200–211. doi:https://doi.org/10.1029/2018EA000493.

[26] R.H. White, R. Toumi, The limitations of bias correcting regional climate model inputs, Geophys. Res. Lett. 40 (2013) 2907–2912. doi:https://doi.org/10.1002/grl.50612.

[27] R. Atlas, R.N. Hoffman, J. Ardizzone, S.M. Leidner, J.C. Jusem, D.K. Smith, D. Gombos, A Cross-calibrated, Multiplatform Ocean Surface Wind Velocity Product for Meteorological and Oceanographic Applications, Bull. Am. Meteorol. Soc. 92 (n.d.) 157–174. doi:https://doi.org/10.1175/2010BAMS2946.1.

[28] M.A. Lackner, A.L. Rogers, J.F. Manwell, J.G. McGowan, A new method for improved hub height mean wind speed estimates using short-term hub height data, Renew. Energy. 35 (2010) 2340–2347. doi:https://doi.org/10.1016/j.renene.2010.03.031.

[29] J.F. Manwell, J.G. McGowan, A.L. Rogers, Wind energy explained: theory, design and application, John Wiley & Sons, 2010.

[30] V.D. Quang, V.Q. Doan, V.N. Dinh, N.D. Duc, Evaluation of resource spatial-temporal variation, dataset validity, infrastructures and zones for Vietnam offshore wind energy, Vietnam J. Sci. Technol. Eng. Vol 62 No 1. (2020). https://vietnamscience.vjst.vn/index.php/VJSTE/article/view/288.

[31] T. Lorenz, I. Barstad, A dynamical downscaling of ERA-Interim in the North Sea using WRF

with a 3 km grid—for wind resource applications, Wind Energy. 19 (2016) 1945–1959.

[32] A.A. Teyabeen, F.R. Akkari, A.E. Jwaid, Power Curve Modelling for Wind Turbines, in: 2017 UKSim-AMSS 19th Int. Conf. Comput. Model. Simul., 2017: pp. 179–184. doi:10.1109/UKSim.2017.30.

[33] GE Renewable Energy, Haliade-X offshore wind turbine, (n.d.). https://www.ge.com/renewableenergy/wind-energy/offshore-wind/haliade-x-offshore-turbine.

[34] C. Desmond, J. Murphy, L. Blonk, W. Haans, Description of an 8 MW reference wind turbine, J. Phys. Conf. Ser. 753 (2016) 92013. doi:10.1088/1742-6596/753/9/092013.

[35] S. Tao, A. Feijóo, J. Zhou, G. Zheng, Topology Design of an Offshore Wind Farm with Multiple Types of Wind Turbines in a Circular Layout, Energies . 13 (2020). doi:10.3390/en13030556.

[36] V.N. Dinh, H.X. Nguyen, Design of an Offshore Wind Farm Layout BT - Proceedings of the 1st Vietnam Symposium on Advances in Offshore Engineering, in: M.F. Randolph, D.H. Doan, A.M. Tang, M. Bui, V.N. Dinh (Eds.), Springer Singapore, Singapore, 2019: pp. 233–238.

[37] P. Reiter, O. Gutjahr, L. Schefczyk, G. Heinemann, M. Casper, Bias correction of ENSEMBLES precipitation data with focus on the effect of the length of the calibration period, Meteorol. Zeitschrift. (2016) 85–96.

[38] L. Trinh-Tuan, J. Matsumoto, F.T. Tangang, L. Juneng, F. Cruz, G. Narisma, J. Santisirisomboon, T. Phan-Van, D. Gunawan, E. Aldrian, T. Ngo-Duc, Application of Quantile Mapping bias correction for mid-future precipitation projections over Vietnam, Sci. Online Lett. Atmos. 15 (2019) 1–6. doi:https://doi.org/10.2151/sola.2019-001.